SAND98-2310J

Contact Hysteresis and Friction of Alkanethiol SAMs on Au

J.D. Kiely and J.E. Houston

Surface and Interface Sciences Department

Sandia National Laboratories

Albuquerque, NM 87185-1413

ABSTRACT

Nanoindentation has been combined with nanometer-scale friction measurements to identify dissipative mechanisms responsible for friction in hexadecanethiol self-assembled monolayers on Au. We have demonstrated that friction is primarily due to viscoelastic relaxations within the films, which give rise to contact hysteresis when deformation rates are within the ranges of 5 and 200 Å/s. We observe that this contact hysteresis increases with exposure to air such that the friction coefficient increases from 0.004 to 0.075 when films are exposed to air for 40 days. Both hysteresis and friction increase with probe speed, and we present a model of friction that characterizes this speed dependence and which also predicts a linear dependence of friction on normal force in thin organic films. Finally, we identify several short-term wear regimes and identify that wear changes dramatically when films age.

INTRODUCTION

The study of friction is fundamentally the study of the mechanisms by which energy is dissipated when two bodies slide past one another. These mechanisms depend upon the stress regime [1] and range from plastic deformation and fracture at very high repulsive stresses [2] to the subtle realignment of molecules as they stretch to make chemical

DISCLAIMER

DISCLAIMER

Portions of this document may be illegible in electronic image products. Images are produced from the best available original document.

bonds with one another at small attractive forces [3]. Within these extremes, many different mechanisms contribute to tribological properties and, if operative mechanisms can be identified and controlled, improvements in friction and wear behavior can be achieved.

Because of their potential as lubricants in nanoscale devices, molecularly thin organic films (liquid and solid) have received considerable attention in tribological studies (see [1,4,5] for reviews). One class of these films, self-assembling organic monolayers, have an added attraction in that by altering chemistry, physical properties may be changed, such that films may be tailored for specific applications [6]. As an example of this, molecular tail groups have been altered to vary adhesive energies [7,8] and frictional properties [9-11]. In self-assembled monolayer systems, many of which are highly ordered, one characteristic that has been associated with friction is the degree of disorder [12-14]. The degree of disorder depends upon the molecule length [15], and friction forces have been inversely correlated with chain length [12-14].

The goal of this research was to identify dissipative mechanisms in a self-assembled monolayer of hexadecanethiol. It has been recognized that dissipation occurring during a cycle of contact and compression is directly related to friction [1]. We will make the same correlation among properties of monolayers when compressed between a smooth asperity and an atomically-smooth surface. In order to clearly identify dissipation mechanisms, we have used an Interfacial Force Microscope (IFM) to quantify forces and hysteretic behavior in the monolayers during a loading cycle (loading to some compressive force and then reversing). We will demonstrate that by combining nanoindentation and friction experiments, viscoelastic dissipation mechanisms can be quantified, and will show that friction in this system is dominated by contact hysteresis of the monolayer. Additionally, we will identify several factors (film age, rate of deformation, and wear history) that influence energy dissipation.

EXPERIMENTAL PROCEDURES

Measurements were performed using the Interfacial Force Microscope (IFM). This instrument, which has been described in detail elsewhere [16], is distinguished by its use of a novel electrostatically-driven feedback sensor to ensure rigid displacement control during a loading experiment. Rigid displacement control ensures that instrument compliance (common in many indentation studies) does not exist, which simplifies analysis of loading cycles. In contrast to other nanoindentation instruments, there is no 'snap-to-contact' instability when using the IFM; the instrument maintains equilibrium by electrostatically balancing the applied force, which keeps the sensor in the same position. This characteristic of the sensor can be exploited to quantitatively map forces throughout attractive and repulsive force regimes. In addition, the IFM has the capability to perform constant-force imaging, similar to other scanning force techniques. Imaging at a low force (0.2 μN) allowed us to quantify damage resulting from our measurements.

Although the IFM was developed to measure forces while moving a probe normal to a surface, it may also be used to measure forces when sliding a probe along the surface. The importance of this is that if the sensor and probe geometry are known, frictional forces and normal forces can be quantified simultaneously. The force sensor maintains a balance of torques, such that while the probe tip is in contact with the sample, if the probe is moved laterally, an additional torque is developed due to the lateral friction force on the probe tip. To maintain a constant sum of all torques, the feedback must change the normal force, which it does by increasing or reducing the depth of deformation. When moving the probe tip laterally in opposing directions, torques developed have opposing senses, which means that the depth of deformation must be increased when the probe moves in one direction and decreased when moving in the opposite direction. The result of this is a friction loop, as illustrated in Fig. 1. When moving to the left (upper portion of the loop) the depth of deformation was reduced (to lower the torque due to the normal force) and when moving to the right the depth of deformation was increased. In order to quantify the friction force that

results in a friction loop, the sensor and probe geometry must be known, as well as the change in normal force with depth of deformation.

To determine this relationship, nanoindentation loading cycles must be performed using the same experimental setup (sensor, probe, and sample). An example of a loading cycle is shown in Fig. 2, along with a fit to the data using Hertzian theory [17]. The Hertzian relationship for a parabolic probe contacting a planar surface is given by the expression [17],

$$F = \frac{4}{3} E^* \sqrt{R}\, \delta^{3/2} \tag{1}$$

where F is the applied force, R is the radius of curvature, δ is the depth of deformation, and E* is the composite modulus, given by

$$\frac{1}{E^*} = \frac{\left(1-\nu_{Au}^2\right)}{E_{Au}} + \frac{\left(1-\nu_W^2\right)}{E_W}, \tag{2}$$

where E_{Au}, E_W, ν_{Au}, and ν_W refer to the elastic modulus and Poisson's ratio of Au and W. Because of the good agreement with the Hertz model, we can confidently use a simple analytic expression (Eq. 1) to relate the depth of deformation to the normal force. With a known change in normal force during a friction loop, and known sample-probe geometry, we can estimate the frictional force.

The force sensor and piezo actuators were calibrated using a standard laboratory electronic balance and a displacement indicator, respectively. Both calibrations are necessary for quantitative measurements. Probes used in this study were electrochemically etched 100 μm tungsten wires with tip radii and parabolic shape determined by field

emission Scanning Electron Microscopy. Au samples with (111)-oriented facets were prepared from 99.99% pure Au wire by flame annealing [18,19]. Immediately after preparation, samples were immersed in a 0.5 mM ethanolic hexadecanethiol ($CH_3(CH_2)_{15}SH$) solution for 24 hr to develop a self-assembled monolayer (SAM) of hexadecanethiol. Samples were dried in N_2, and were mounted for IFM interrogation, which was performed in air but under a cover to prevent exposure to light. Unless otherwise noted, the rate of displacement for force profiles was 10 Å/s and the lateral speed during a friction trace was 100 Å/s.

RESULTS

To investigate how the mechanical properties of the monolayer degrade over time, force profiles were acquired from new samples (0-2 days old) and from samples that had been exposed to air for 40 - 45 days. A force profile typical of new monolayer behavior is presented in Fig. 3a. Data from the loading segment of the loading cycle is marked by open circles and the unloading segment by closed circles. Force profiles from new samples showed virtually no hysteresis, indicating that little energy was dissipated during a loading cycle (loading and unloading). Fig. 3c illustrates the dependence of friction on normal force for new monolayers. Below a normal force of ~4 μN, which corresponds to a mean normal stress of ~3.7 GPa (calculated using Hertzian mechanics), friction is minimal. The coefficient of friction was quantified by a least-squares linear fit to be approximately 0.004. Above 3.7 GPa it increased to 0.12. It was observed that measuring friction in this high-stress regime damaged the monolayer (a depression several Å deep was observed), so it is likely that the increase in friction is due to dissipation through increasing damage (discussed in more detail below). Note that in both stress regimes, the dependence of friction on normal force was roughly linear, which allows us to a friction coefficient for this particular tip speed. When normal forces were further increased such that stresses

were above 5 – 6 GPa, plastic deformation of Au was observed, and friction coefficients were much higher.

The behavior of aged monolayers was markedly more hysteretic. A force profile typical of an aged monolayer is presented in Fig. 3b and demonstrates this increased hysteresis. During the loading portion of the cycle, repulsive forces were observed over a longer range than seen in new samples, and the force dropped to zero more rapidly during unloading. Note that this hysteresis is not due to an increase in adhesion (which would be observed as negative forces), but due to a change in the time dependence of repulsive forces. The corresponding friction response is shown in Fig. 3d. Except for normal forces less than 1 μN, the friction force is again a linear function of the applied force, with a coefficient of friction of 0.075. This is an increase in friction coefficient over that of a new monolayer of more than an order of magnitude and demonstrates that an increase of contact hysteresis correlates with an increase in friction.

The stresses used in this study were high (> 1 GPa), and a question that arises is whether friction forces changed with repeated measurement, i.e., does the film 'wear'? For new monolayers, force profiles and friction loops repeated in the same location remained unchanged unless stresses were above 3.5 - 4 GPa. Above this threshold, a depression several Å deep , i.e., a 'wear track', was observed. Thus, new monolayers showed higher friction only when damaged. Aged monolayers, on the other hand, showed noticeable wear at all stresses. Fig. 4a illustrates the decrease in friction force as the same section of the sample is repeatedly probed. It decreases over the first 20-30 cycles to roughly 70% of the initial friction force ($F_{\mu,i}$). A force profile taken after 30 cycles is shown in Fig. 4b, and when compared to that of undamaged monolayer (shown by the broken line), a reduction in the amount of hysteresis is observed. A depression approximately 10 Å deep (a 'wear track') was also observed after 30 cycles, indicating that aged monolayers can be worn by repeated deformation.

To better understand the relationship between the friction and contact hysteresis of aged films, we varied the speed at which nanoindentation and friction properties were investigated. We have related lateral (v_X) and vertical (v_Z) velocities using a simple model for the distance near the contact periphery within which the monolayer will be fully compressed. Since our depths of contact were much greater than the film thickness, we find that compression should occur over a distance of 12 h, where h is the film thickness, giving $v_X \approx 0.08\ v_Z$. Correlations between nanoindentation and friction properties over a range of speeds are presented in Fig. 5. Fig. 5a presents F_μ/F_N as a function of v_X for aged monolayers that have not been worn (i.e., initial friction traces were analyzed). A strong speed dependence exists, with F_μ/F_N increasing with v_X. Force profiles were acquired at rates of $v_Z = 5$, 20 and 200 Å/s and we present loading and unloading portions of these data separately. Loading portions of these cycles are presented in Fig. 5b. At a displacement rate of 200 Å/s, the monolayer initially supports higher stresses than it does when compressed at 5 or 20 Å/s, which results in greater nanoindentation hysteresis and greater friction. Unloading portions are presented in Fig. 5c, and while there appears to be little difference between unloading at 20 and 200 Å/s, unloading at 5 Å/s results in repulsive forces over a longer range, which translate into lower hysteresis and lower friction. Nanoindentation displacement rates of 5, 20, and 200 Å/s correspond to friction measurements at 63, 250, and 2500 Å/s, which have been identified by open triangular markers on the abscissa of Fig. 5a. Thus, there is good correlation between the increase in friction and the increase in contact hysteresis with speed.

DISCUSSION

We have presented three examples of the correlation between contact hysteresis and friction, each of which demonstrate the benefit of having a versatile, mechanically stable force sensor that can quantify normal and lateral forces. It has enabled us to characterize contact hysteresis and adhesion independently, such that we have observed hysteresis in

the absence of adhesion (see Fig. 2-5). We will first comment on the observation of a linear dependence of friction on normal force and then discuss the processes responsible for the age, wear, and speed dependence of friction.

Linear dependence of friction on normal force

Others [10,12,13] and we have found that for organic monolayer films, F_μ increases roughly linearly with F_N in the repulsive loading regime at high stresses. This contrasts with measurements of organic films [1,12] and clean contacts [20] that indicate that friction is a non-linear function of the applied force when forces are low. Because the stresses used in this study are high and the adhesive energy of the methyl-terminated alkanethiol film is low[7], we believe that dissipation due to compressing the monolayer dominates that due to the adhesion-related hysteresis. Starting with this assumption and using a viscoelastic model of the monolayer, we show in the following why F_μ increases linearly with F_N.

To understand why friction forces vary linearly with normal force, we start with the assumption that the deformation of alkanethiol monolayers can be described using linear viscoelasticity [21,22]. Following Persson [23], we approximate the monolayer using the standard linear solid model (a spring in series with a Voigt element that has a spring constant E_o and a relaxation time constant τ_o). Additionally, we approximate our loading (during both a force profile and a friction measurement) as sinusoidal loading with a peak stress σ_o and a frequency ω. Although we measure losses from only a portion of such a loading cycle (our probe would have to be bonded to the surface to apply both tensile and compressive stresses), this should illustrate the dominant characteristics of the system. Under cyclic stressing, the absorbed energy density is [24]:

$$U = \frac{\pi\sigma_o^2}{E_o}\frac{\omega\tau_o}{1+\omega^2\tau_o^2}. \qquad (3)$$

This can be related to friction by considering the work required to move the probe against the friction force over some distance d:

$$W_\mu = F_\mu d. \tag{4}$$

This work is also the energy absorbed by the film, which is the energy density (Eq. 3) times the volume of the film compressed during movement:

$$W_\mu = U \cdot 2adh, \tag{5}$$

where a is the contact radius and h is the film thickness. Thus,

$$F_\mu = \frac{\pi\sigma_o^2}{E_o}\frac{\omega\tau_o}{1+\omega^2\tau_o^2}\cdot 2ah. \tag{6}$$

The stress is given by

$$\sigma = \frac{F_N}{\pi a^2}, \tag{7}$$

and since $a = \left(\frac{3F_N R}{4E^*}\right)^{1/3}$ 17,

$$F_\mu = \frac{4E^* F_N}{3\pi E_o R}\frac{\omega\tau_o}{1+\omega^2\tau_o^2}\cdot 2h. \tag{8}$$

Thus, we expect friction in a thin viscoelastic film to be linearly dependent upon normal load. Additionally, this result is not limited by the single relaxation model used; we expect a linear dependence even in the more realistic case of a spectrum of relaxation time constants.

It is worthwhile to point out how different sample configurations give rise to different scaling behavior between friction and normal forces. From the above, we expect friction forces to be linearly dependent on the normal force when a thin (h << a) layer is investigated with a spherical probe. If the layer were not thin, the volume that dissipates energy in Eq. 5 would be $\pi a^2 d/2$, and we'd expect $F_\mu \propto F_N^{4/3}$, as is reported for many bulk measurements [2,17]. Alternatively, if a flat, cylindrical punch were used to characterize a thin layer, the contact radius would be independent of F_N, and we'd expect $F_\mu \propto F_N^{2/3}$. Thus, the functional dependence of F_μ on F_N is specific to the experimental arrangement.

We can alternatively consider friction in terms of an interfacial shear strength,

$$\tau_\mu = \frac{F_\mu}{\pi a^2} \propto F_N^{1/3}. \tag{9}$$

Since the applied stress, also scales as $F_N^{1/3}$, we observe that $\tau_\mu \propto \sigma$, which is consistent with the general description of τ_μ [2]:

$$\tau_\mu = \tau_o + \mu\sigma. \tag{10}$$

This simply means that τ_o is low in our experiments, which is consistent with our observations of very low adhesion. This description of the interfacial shear strength is very general and has been applied to friction when plastic deformation of metals is involved [2], in the very high stress regime (the 'cobblestone' model) [1], and for Langmuir-Blodgett monolayer films on mica [25]. A pressure-dependent interface shear strength has been

observed in systems of thin organic films [4], and has been observed for alkanethiol monolayers via atomistic simulations [26].

Speed Dependence of Friction in Aged Films

Using the above framework, we can rationalize our observed speed dependence of friction. We have assumed a single relaxation time constant, even though it is known that viscoelastic behavior is typically described by a relaxation spectrum [27]. The relaxation spectrum of the monolayer is a signature of the molecular relaxation mechanisms occurring [27,28]. For alkanethiol monolayers, one important mechanism is the change in tilt angle of molecular chains [26]. It is believed that loading cycles produce a cycle in tilt angle and that the characteristic time constant of the tilt restoring force directly relates to the observed hysteresis. Although the simplicity of our single-relaxation approach precludes a complete description of loss mechanisms in these films, it does give some insight into our observations.

From Eq. 8, we find that $\frac{F_\mu}{F_N} \propto \frac{\omega\tau_o}{1+\omega^2\tau_o^2}$. This implies that at increasing frequencies, friction rises and peaks when $\omega\tau_o = 1$. We have measured friction as a function of tip speed, which can be related to a frequency through some characteristic distance. As stated above, we've used a simple geometrical model for the compression of the film and find that it should occur over a distance of about 12h. Using $\omega \approx 12h/v_x$, we find that $\frac{F_\mu}{F_N} \propto \frac{h\tau_o v_x}{v_x^2+h^2\tau_o^2}$, which peaks at $v_x = 12h\tau_o$.

The relaxation response of aged hexadecanethiol films has been measured, giving a single time constant of 0.08 s [21]. Using 20Å as the monolayer thickness, the maximum loss for this relaxation should occur around 3000 Å/s. Our experimental findings, that

friction rises throughout our experimental speed range, indicates that the peak is well above 2000Å/s, which is consistent with this prediction. Our speed range is limited by the apparatus configuration, and we cannot presently measure friction at higher speeds.

Although time constants are best measured by instantaneously imposing a stress or strain and monitoring the relaxation [21], we can draw some conclusions about relaxations in the film by performing loading cycles at various speeds. During loading of an aged film (Fig. 5b), there appears to be a relaxation rate between 20 and 200 Å/s. Force-deformation relationships are nearly identical for 5 and 20 Å/s, but increasing the displacement rate to 200 Å/s results in higher forces for equivalent deformations. A relaxation rate between 20 and 200 Å/s translates to a time constant between 0.1 and 1 s. However, there appears to be a separate time constant for retraction. In Fig. 5c, retracting the tip at 20 or 200 Å/s results in stresses dropping to zero within the first several Å of movement. When retracting the tip at 5 Å/s, the monolayer can at least partially relax, which is observed by a repulsive force that decreases to zero over approximately 15 Å. Thus, relaxation occurs at a rate somewhere between 5 and 20 Å/s, giving a time constant between 1 and 4 s. These longer time constants indicate that multiple relaxation rates do exist in aged films and that friction is speed dependent even at the lower limits of scanning capabilities.

Monolayer aging and wear

Details of monolayer deformation have been investigated via both experimentation [21] and atomistic simulation [26,29], which provide the basis for an understanding of how aging increases contact hysteresis. Unstressed self-assembled hexadecanethiol monolayers have a tilt angle from the surface normal (θ) of roughly 30° [6,15,29]. Molecular dynamics simulations of uniform compression of this system indicates that compression involves three structural changes [26]: the tilt angle of the molecules increases to a maximum of 48°, bonds within the chains are elastically compressed, and a structural transition, whereby

some of the sulfur head groups shift from three-fold hollow to two-fold bridge sites, occurs. These changes were all found to be reversible, and, in a study of the tribological properties of this system, the primary dissipation mechanism was oscillation of the tilt angle of the alkyl chains, resulting in a friction coefficient of < 0.02 for two contacting monolayers [26]. Our results on the friction coefficient and the amount of hysteresis in new monolayers are consistent with these predictions, and we take the view that changes in friction and hysteresis are due to changes in the freedom of movement of alkyl chains.

It has been established that lower packing density is associated with higher friction [12,13]. Interchain interactions dominate the energetics of monolayer compression [29], so that with high packing density, alkyl chains move in concert [29]. With low packing density, the movement of each chain is less dependent upon that of its neighbors, so that compression of the film can involve less concerted movement of chains. Compression of a less ordered film involves non-uniform changes in tilt angle and the formation of gauche defects [30]. Since vibrational chain movement is the dominant mechanism of dissipation [26] and less ordering increases freedom of chain movement, if reduced packing density occurs during aging, we expect higher friction.

The aging of hexadecanethiol monolayers in air has been associated with ozonolysis [31]. An increase in θ [32], fragmentation of the alkyl chain [33], and the oxidation of thiolate species to sulfonate species [34] have been observed during aging. It is also believed that aging involves an increase in disorder [35]. The causes of disordering may be the incorporation of oxygen into the adsorbed sulfur layer or the reduction in interchain interactions resulting from chain fragmentation, but regardless of which mechanism leads to disorder or lower packing density, it is clear that the changes taking place result in greater friction and hysteresis.

We also observed strong wear behavior in aged films. Scanning repeatedly reduced contact hysteresis and friction and resulted in a depression in the film. There appeared to

be transient and steady-state components to both the contact hysteresis and friction in that hysteresis and friction decreased over the first 30 cycles, but persisted after many more. Additionally, we observed the cessation of the transient component to coincide with attaining the limit of film damage (10 Å). With a reduced film thickness, we attribute the reduction in friction during wear to a reduction in the volume of material that can dissipate mechanical energy. An alternate possibility is that wearing the film also involves a reordering once the thickness has been reduced. It is important to point out, however, that 1) friction after wearing the film is still much greater than in new monolayers and 2) even after repeated wear at high stresses and after plastic deformation of the Au substrate, the film still passivates the probe-sample interaction.

We consider two damage mechanisms: the removal of a fraction of the monolayer and the fragmentation of alkyl chains. Regarding the first, sulfonates bind more weakly to Au than thiolates [36,37] to the degree that one method of patterning films is through oxidation and rinsing in an alcohol [37]. In non-oxidized films, a reversible structural transition in thiolate ordering has been observed at high stresses [12,29,38], so we expect reversible thiolate displacement to occur in our non-oxidized films. The lower binding energy of the sulfanotes in oxidized films makes displacement more likely at lower stresses and may lead to irreversibilty in the transition or to sulfonate removal. In this case, wearing the film would involve removal of a certain fraction of sulfonate species and the attached alkyl chains. Fragmentation of alkyl chains is reported to be aided by the oxidation process [33] and the act of measuring friction may remove the fragmented species. The high stresses may also fragment additional chains. Both mechanisms would give rise to the observed behavior, and with either the loss of a fraction of sulfonates or fragmentation of alkyl chains, we expect a reduction in the volume available to dissipate mechanical energy and a corresponding reduction in friction.

CONCLUSIONS

We have developed a technique that permits the direct comparison of friction and mechanical properties on the nanometer scale. We have applied this technique to investigate the sources of friction in self-assembled monolayers of hexadecanethiol and have observed a strong correlation between contact hysteresis and friction. In all monolayers, friction forces increased linearly with applied normal force, allowing us to characterize friction using a coefficient. Contact hysteresis and friction were observed to increase with age, and we propose that aging of the film results in a reduction in packing density when stressed, which leads to greater chain mobility and more modes of energy dissipation. Additionally, we have identified that aged films wear rapidly at high stresses and have identified the dependence of friction on rate of deformation. These results indicate that the age and storage of these materials must be taken into account when tribological properties are investigated.

ACKNOWLEDGMENTS

The authors would like to thank R.W. Carpick for helpful discussions. This work was supported by the U.S. Department of Energy under Contract DE-AC04-94AL85000. Sandia is a multiprogram laboratory operated by Sandia Corporation, a Lockheed-Martin Company, for the U.S. Department of Energy.

FIGURE CAPTIONS

Fig. 1 Typical friction loop from an IFM friction experiment. Friction forces give rise to additional torques on the sensor, for which the feedback compensates by increasing or reducing the torque due the normal force (i.e. changing the depth of deformation). Moving to the left, feedback retracted the tip from the sample and moving to the right, it increased the depth of deformation.

Fig. 2 Loading cycle demonstrating near-elastic behavior of monolayer-Au couple. Data shows a very good fit to the Hertzian model, which is used to estimate the change in normal force with change in tip vertical position.

Fig. 3 Correlation between contact hysteresis and friction. (a) Loading cycle demonstrating the minimal contact hysteresis of a monolayer 0-2 days old. (b) Loading cycle of a film that was exposed to air for 40 days. A distinct increase in hysteresis is observed in the aged monolayer. (c) Friction force as a function of normal force for a new monolayer. Friction is minimal. (d) Friction vs. normal force for the aged monolayer. Friction forces rise linearly with normal force at a much greater rate than for new monolayers.

Fig. 4 (a) Normalized friction coefficient as a function of number of measurement cycles in the same location for aged films. The friction force (F_μ) is normalized by that of the first measurement cycle ($F_{\mu,i}$). Friction forces drop to ~ 75% of their original value over 20 - 30 cycles. (b) The change in contact hysteresis with wear. The behavior of the monolayer after thirty wear cycles is shown and, for comparison, behavior of an unworn, aged monolayer is shown by the broken line. The reduction in contact hysteresis with wear correlates with the reduction in friction.

Fig. 5 (a) Dependence of the normalized friction force on lateral tip speed (v_x), quantifying the increase in friction with deformation rate for an aged film. Error bars represent scatter in the measurements. The open arrows along the abscissa identify the lateral velocities (62.5, 250, and 2500 Å/s) that roughly correspond to v_z = 5, 20 and 200 Å/s. (b) Loading portion of loading cycles at three speeds. Force-deformation relationships appear to be the same for deformation rates of 5 and 20 Å/s, but the film appears stiffer at 200 Å/s. (c) Unloading portion of loading cycles at three speeds. At 5 Å/s, recovery of the monolayer is observed, while at 20 and 200 Å/s, virtually no relaxation is observed.

REFERENCES

1)Israelachvili, J. N. *CRC Handbook of Micro/Nano Tribology*; Bhushan, B., Ed.; CRC Press: Boca Raton, 1995, pp 267.

2)Bowden, F. P.; Tabor, D. *The Friction and Lubrication of Solids: Part II*; Clarendon Press: Oxford, 1964.

3)Burns, A. R.; Houston, J. E.; Carpick, R.; Michalske, T. E. *Phys. Rev. Lett.* **1998.**

4)Carpick, R. W.; Salmeron, M. *Chem. Rev.* **1997**, *97*, 1163-1194.

5)Colton, R. J. *Langmuir* **1996**, *12*, 4574-4582.

6)Ulman, A. *Chem. Rev.* **1996**, *96*, 1533-1554.

7)Thomas, R. C.; Houston, J. E.; Crooks, R. M.; Kim, T.; Michalske, T. A. *J. Am. Chem. Soc.* **1995**, *117*, 3830.

8)Ulman, A.; Evans, S. D.; Shnidman, Y.; Sharma, R.; Eilers, J. E.; Chang, J. C. *J. Am. Chem. Soc.* **1991**, *113*, 1499.

9)Noy, A.; Frisbie, C. D.; Rozsnyai, L. F.; Wrighton, M. S.; Lieber, C. M. *J. Am. Chem. Soc.* **1995**, *117*, 7943-7951.

10)Kim, H. I.; Koini, T.; Lee, T. R.; Perry, S. S. *Langmuir* **1997**, *13*, 7192.

11)Tsukruk, V. V.; Everson, M. P.; Lander, L. M.; Brittain, W. J. *Langmuir* **1996**, *12*, 3905-3911.

12)Lio, A.; Charych, D. H.; Salmeron, M. *J. Phys. Chem. B* **1997**, *101*, 3800-3805.

13)McDermott, M. T.; Green, J.-B. D.; Porter, M. D. *Langmuir* **1997**, *13*, 2504-2510.

14)Xiao, X.; Hu, J.; Charych, D. H.; Salmeron, M. *Langmuir* **1996**, *12*, 235-237.

15)Porter, M. D.; Bright, T. B.; Allara, D. L.; Chidsey, C. E. D. *J. Am. Chem. Soc.* **1987**, *109*, 3559-3568.

16)Joyce, S. A.; Houston, J. E. *Review of Scientific Instruments* **1991**, *62*, 710-715.

17)Johnson, K. L. *Contact Mechanics*; Cambridge University Press: Cambridge, 1996.

18)Hsu, T.; Cowley, J. M. *Ultramicroscopy* **1983**, *11*, 239.

19)Schneir, J.; Sonnenfeld, R.; Marti, O.; Hansma, P. K.; Demuth, J. E.; Hamers, R. J. *J. Appl. Phys.* **1988**, *63*, 717-721.

20)Carpick, R. W.; Agraït, N.; Ogletree, D. F.; Salmeron, M. *J. Vac. Sci. Technol. B* **1996**, *14*, 1289-1295.

21)Joyce, S. A.; Thomas, R. C.; Houston, J. E.; Michalske, T. A.; Crooks, R. M. *Physical Review Letters* **1992**, *68*, 2790-2793.

22)Salmeron, M.; Neubauer, G.; Folch, A.; Tomitori, M.; Ogletree, D. F.; Sautet, P. *Langmuir* **1993**, *9*, 3600-3611.

23)Persson, B. N. J. *Sliding Friction*; Springer: Berlin, 1998.

24)Williams, J. G. *Stress Analysis of Polymers*; 2nd ed.; Ellis Horwood Limited: Chichester, 1980.
25)Briscoe, B. J.; Evans, D. C. *Proc. Roy. Soc. London* **1982**, *A380*, 389-407.
26)Tupper, K. J.; Brenner, D. W. *Thin Solid Films* **1994**, *253*, 185-189.
27)Ferry, J. D. *Viscoelastic Properties of Polymers*; John Wiley & Sons: New York, 1980.
28)McCrum, N. G.; Read, B. E.; Williams, G. *Anelastic and Dielectric Effects in Polymeric Solids*; Dover Publications: New York, 1991.
29)Tupper, K. J.; Brenner, D. W. *Langmuir* **1994**, *10*, 2335-2338.
30)Tupper, K. J.; Colton, R. J.; Brenner, D. W. *Langmuir* **1994**, *10*, 2041-2043.
31)Zhang, Y.; Terrill, R. H.; Tanzer, T. A.; Bohn, P. W. *J. Am. Chem. Soc.* **1998**, *120*, 2654-2655.
32)Horn, A. B.; Russell, D. A.; Shorthouse, L. J.; Simpson, T. R. E. *J. Chem. Soc., Faraday Trans.* **1996**, *92*, 4759-4762.
33)Norrod, K. L.; Rowlen, K. L. *J. Am. Chem. Soc.* **1998**, *120*, 2656-2657.
34)Hutt, D. A.; Leggett, G. J. *J. Phys. Chem.* **1996**, *100*, 6657 -6662.
35)Dishner, M. H.; Feher, F. J.; Hemminger, J. C. *Chem. Comm.* **1996**, 1971-192.
36)Tarlov, M. J.; Newman, J. G. *Langmuir* **1992**, *8*, 1398-1405.
37)Tarlov, M. J.; Burgess, D. R. F., Jr.; Gillen, G. *J. Am. Chem. Soc.* **1993**, *115*, 5305-5306.
38)Liu, G.-y.; Salmeron, M. *Langmuir* **1994**, *10*, 367.

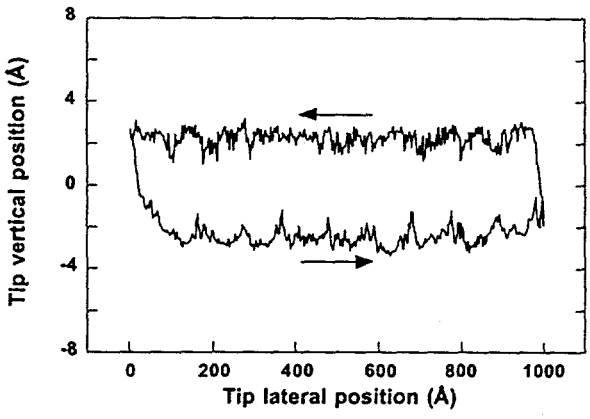
8
4
0
-4
-8
Tip vertical position (Å)
0
200
400
600
800
1000
Tip lateral position (Å)

Fig. 1

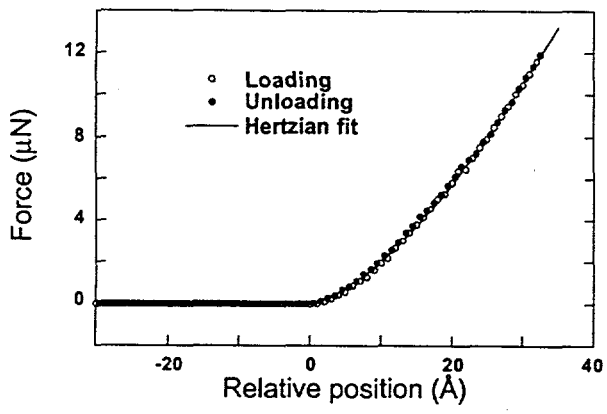
Loading
Unloading
Hertzian fit
Force (μN)
12
8
4
0
-20
0
20
40
Relative position (Å)

Fig. 2

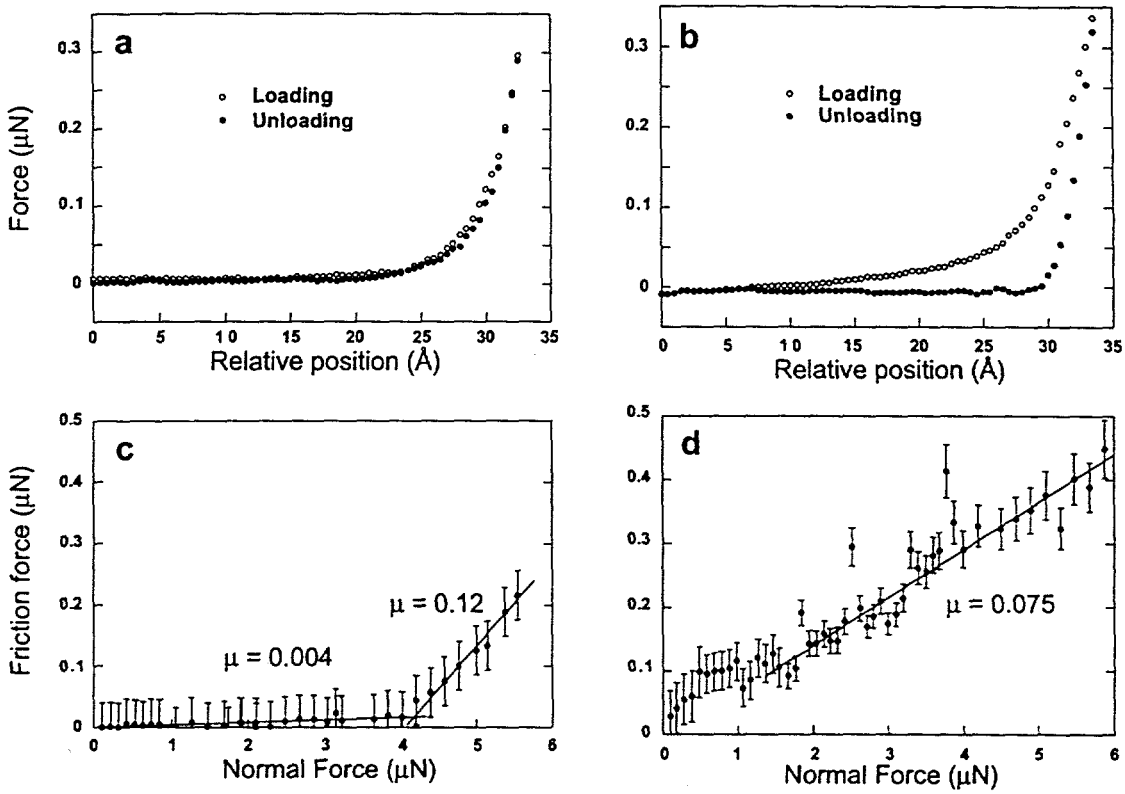
a
Loading
Unloading
Force (μN)
Relative position (Å)
b
Loading
Unloading
Relative position (Å)
c
μ = 0.004
μ = 0.12
Friction force (μN)
Normal Force (μN)
d
μ = 0.075
Normal Force (μN)

Fig. 3

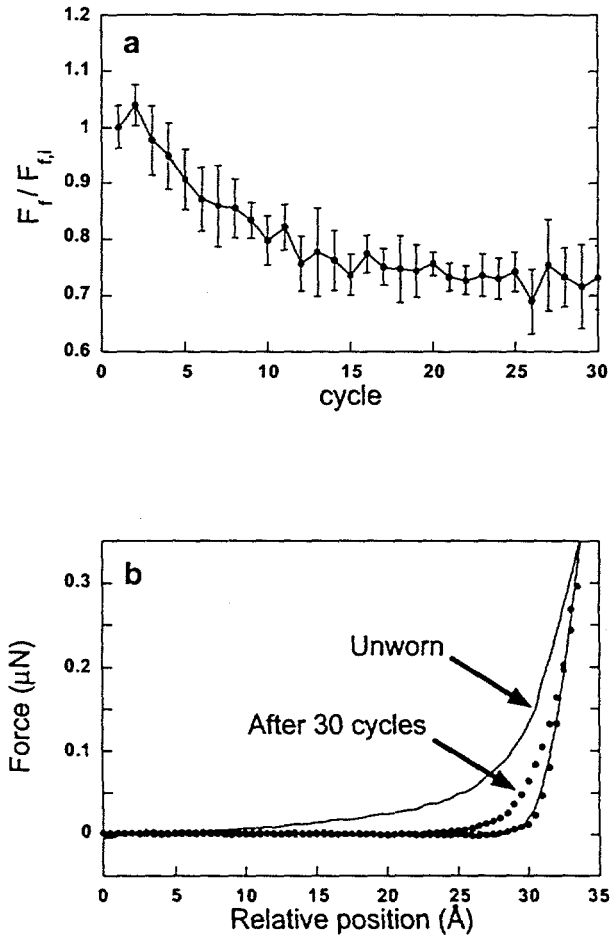
a
1.2
1.1
1
0.9
0.8
0.7
0.6
$F_f / F_{f,I}$
0
5
10
15
20
25
30
cycle
b
0.3
0.2
0.1
0
Force (μN)
Unworn
After 30 cycles
0
5
10
15
20
25
30
35
Relative position (Å)

Fig. 4

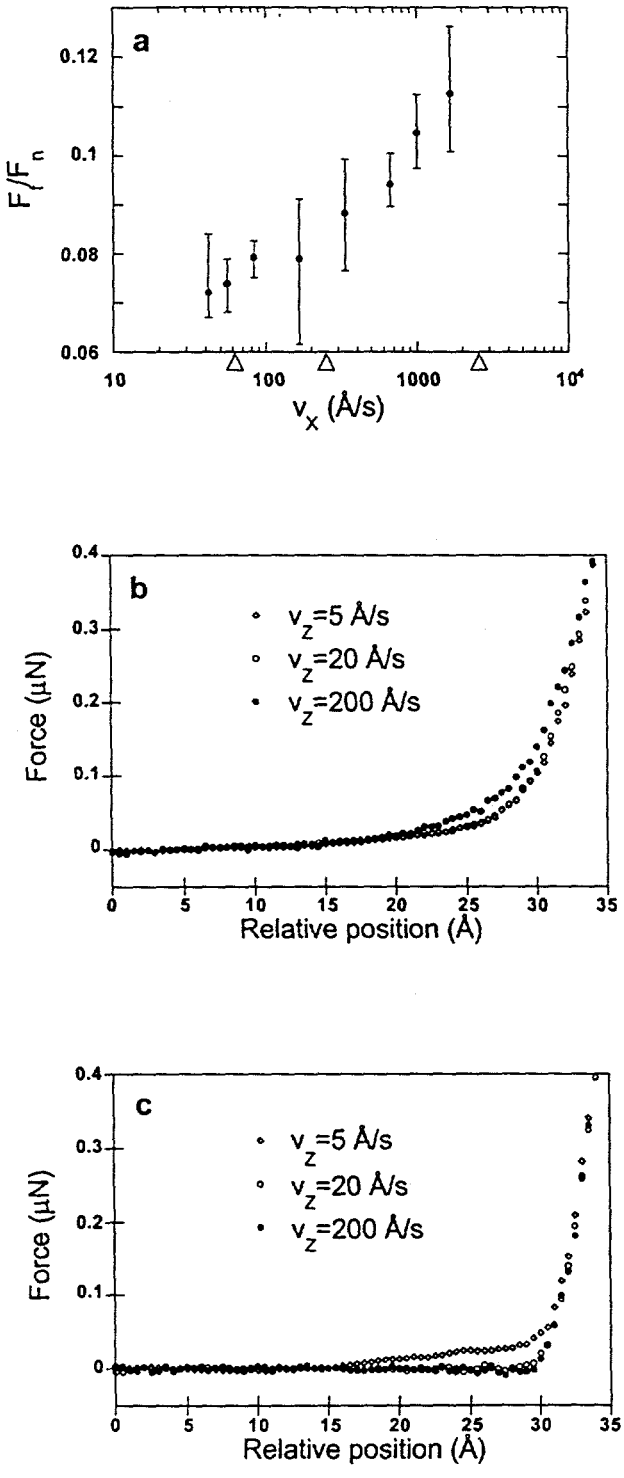
a
0.12
0.1
0.08
0.06
F/F_n
10
100
1000
10^4
v_x (Å/s)
b
v_z=5 Å/s
v_z=20 Å/s
v_z=200 Å/s
Force (μN)
0.4
0.3
0.2
0.1
0
0
5
10
15
20
25
30
35
Relative position (Å)
c
v_z=5 Å/s
v_z=20 Å/s
v_z=200 Å/s
Force (μN)
0.4
0.3
0.2
0.1
0
0
5
10
15
20
25
30
35
Relative position (Å)

Fig. 5

Kiely & Houston
Fig. 5